PROGRESS IN PHOTOVOLTAICS: RESEARCH AND APPLICATIONS, VOL 1, 133–143 (1993)

Research

High-efficiency Silicon Solar Cells: Fill Factor Limitations and Non-ideal Diode Behaviour Due to Voltage-dependent Rear Surface Recombination Velocity

Armin G. Aberle, Stephen J. Robinson, Aihua Wang, Jianhua Zhao, Stuart R. Wenham and Martin A. Green

Centre for Photovoltaic Devices and Systems, University of New South Wales, P.O. Box 1, Kensington NSW 2033, Australia

Despite exceptionally high open-circuit voltages, record high-efficiency PERL (passivated emitter, rear locally diffused) silicon solar cells recently developed at the University ofNew South Wales demonstrate relatively low fill factors. This behaviour is shown to result from a surface recombination velocity at the rear $Si–SiO_2$ interface that increases with reducing voltage across the cell, leading to non-ideal I–V curves with high ideality factors (>1.3) near the maximum power point. When corrected for series resistance losses, the Air Mass 1.5 (AM1.5) fill factor of actual PERL cells is found to be limited to values below 82.9%, as opposed to the ideal theoretical limit of 85–86% for silicon cells operating in low injection conditions. Relatively large series resistance losses ($R_S > 0.35\ \Omega\ cm^2$) further reduce this value to the experimentally observed fill factors below 81.4%.

Analysis of measured illuminated and dark I–V characteristics of PERL cells reveals that the AM1.5 efficiency is mainly limited by recombination losses at the rear oxidized surface. Optimum PERL cell resistivity is about 2 Ω cm. Owing to increased rear surface recombination velocity, lower resistivity material shows no advantage in open-circuit voltage and suffers from short-circuit current losses, while a strong reduction in the surface recombination velocity above the maximum power point results in smaller fill factors. High-resistivity cells do show an improved short-cuircuit current but suffer from voltage and fill factor losses.

INTRODUCTION

The passivated emitter, rear locally diffused (PERL) silicon solar cell structure of Figure 1 has recently been developed at the University of New South Wales (UNSW). Owing to improved surface and metal contact passivation and high carrier lifetimes, PERL cells have demonstrated record-high efficiencies above 23% under the global Air Mass 1.5 (AM1.5) spectrum normalized to 100 mW cm^{-2} at 25°C.[1–3] The striking features of the PERL cell structure are a passivating silicon

1062–7995/93/020133–11 $10.50

Received 18 December 1992
Revised 14 January 1993

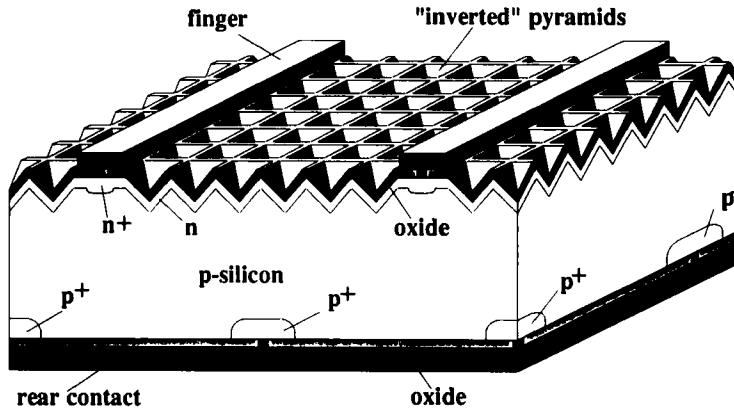

Figure 1. Passivated emitter, rear locally-diffused cell (PERL cell)

dioxide layer on both surfaces, inverted pyramids on the illuminated front surface (for reduced reflection as well as improved light trapping), a lightly diffused phosphorus emitter and heavy, deep diffusions underneath the front and rear metal contacts for low metal contact recombination. To reduce reflection losses, the front surface oxide on the inverted pyramids has a thickness of 1100 Å, while the rear oxide is about 3000 Å thick.

The highest efficiencies to date are obtained with relatively thick (280 μm) and medium resistivity (~2 Ω·cm) p-type float zone (FZ) silicon wafers polished on both sides. At UNSW, two 20 mm × 20 mm cells are located on a 50.8-mm diameter wafer. In order to avoid a small but erratic efficiency loss from laser scribing, the cells usually remain embedded in the wafer and are measured with an opaque 20 mm × 20 mm shading mask. The electrical parameters of one of the best cells (Wb34-R), using presently accepted AM1.5G calibration standards, are: efficiency $\eta = 23.1\%$, open-circuit voltage $V_{oc} = 696$ mV, short-circuit current density $J_{sc} = 40.9$ mA cm^{-2}, fill factor $FF = 81.0\%$. Despite exceptionally high open-circuit voltages, PERL cells demonstrate relatively modest fill factors below 81.4%, compared to earlier generations of UNSW cells that have demonstrated fill factors in the 83–84% range. Substantial improvements in cell efficiency could be achieved if the mechanisms limiting these fill factors could be understood and eliminated.

NON-IDEAL DARK AND ILLUMINATED I–V CHARACTERISTICS

Dark I–V characteristics

Figure 2 shows the measured dark *I–V* characteristics of four PERL cells with a planar front surface. Bulk resistivity ranges from 1 to 100 Ω·cm. The 1 Ω·cm cell exhibits the expected ideal low injection behaviour with a straight line segment of unity ideality factor only for voltages below 400 mV. With increasing voltage, the slope of the dark *I–V* curve decreases until a second straight line segment with a very high ideality factor of about 1.55 is reached. Apart from shunt resistance effects in the 10 and 100 Ω·cm cell, the other cells show very similar behaviour. With increasing base resistivity, however, the saturation current density increases and the deviation from ideal diode behaviour starts at lower voltages.

J_{sc} V_{oc} *characteristics*

The non-ideal behaviour of PERL cells is also found in illuminated measurements, as can most evidently be seen from the J_{sc}–V_{oc} characteristics. To determine this curve, the short-circuit current density J_{sc} and the open-circuit voltage V_{oc} are measured at varying light intensities. Shifting the measured illuminated AM1.5 *I–V* curve by the short-circuit current density from the fourth into the first quadrant allows for

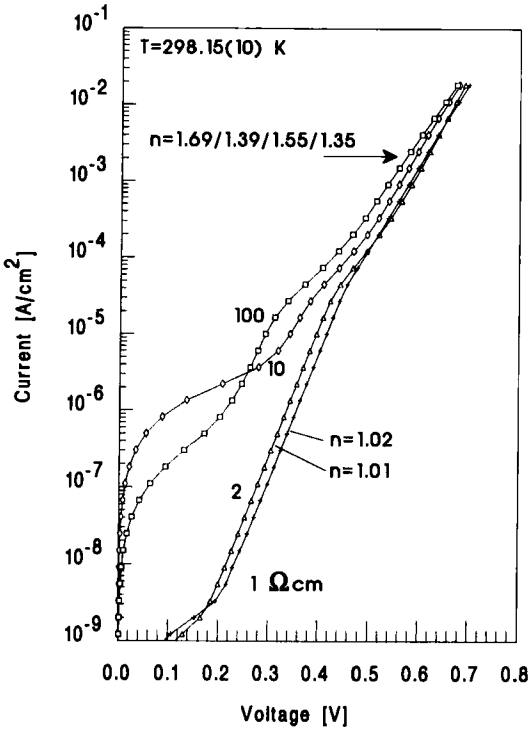

Figure 2. Measured dark I–V characteristics of planar front surface PERL cells with resistivity ranging from 1 to 100 Ω·cm (data points are joined by linear segments for visualization only)

a direct comparison of the J_{sc}–V_{oc} curve and the illuminated I–V curve. As neither the short-ciruit current nor the open-circuit voltage of practical solar cells are affected by series resistance losses, the J_{sc}–V_{oc} characteristics are a first-order approximation to the series resistance-corrected illuminated I–V curve of the device.

Figure 3 shows the measured J_{sc}–V_{oc} characteristics of the four PERL cells of Figure 2 for light intensities from 0.015 to 2 suns. The measured J_{sc}–V_{oc} curves can be separated into three regions: near 700 mV (V_{oc} at 1 sun) the ideality factor of the cells is close to unity, at smaller voltages it is much greater and at larger voltages it is less than one. As will be discussed in the next section, the deviation of the I–V curves from ideal diode behaviour below 700 mV is due to a rear surface recombination velocity that strongly increases with reducing voltage across the cell. The bending of the curves above 700 mV, resulting in apparently less than unity ideality factors, is largely due to an increased cell temperature. The measurements in Figure 3 (as well as all the other illuminated I–V measurements reported in this work) were obtained on the solar simulator located within the Centre for Photovoltaic Devices and Systems at UNSW. The wafers are vacuum-contacted on a 200 mm × 150 mm × 6 mm copper block and cell voltage and current are measured by the four-point probe technique. A silicon wafer with a laser-scribed 20 mm × 20 mm window and a 0.2 μm thick evaporated aluminium layer is used as a shading mask. Block temperature is controlled by a Peltier device and measured by a thermistor contacting the bottom of the block. Temperature uncertainty at the bottom of the block is ±0.2 K near room temperature.

Although the bottom of the copper block was fixed to 25°C in the steady-state measurements of Figure 3, cell temperature was found to increase approximately linearly with light intensity owing to the non-zero thermal resistance between the cell and block. In order to assess the temperature increase we have applied a second measurement technique. In the first step the whole system is shaded and fixed to 25°C.

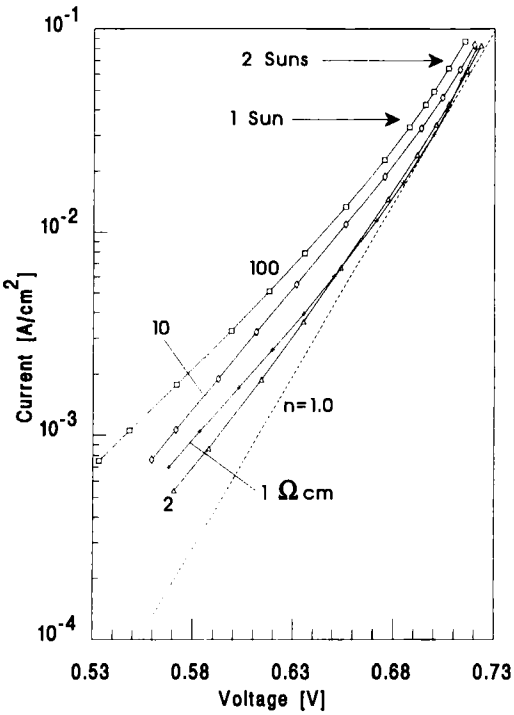

Figure 3. J_{sc}–V_{oc} characteristics of the four cells of Figure 2

Subsequently, the shading plate is quickly removed and the time dependence of V_{oc} (or J_{sc}) is determined with a digital multimeter. Regarding the maximum values as the corresponding open-circuit voltage and short-circuit current at 25°C, respectively, the V_{oc} and J_{sc} deviations of the steady-state technique are found to be adequately described by the linear expressions $\Delta V_{oc} = -1.6 \times 10^{-2} \cdot J_{sc}$ mV and $\Delta J_{sc} = +3.2 \times 10^{-3} \cdot J_{sc}$ mA cm^{-2}, where J_{sc} is measured in mA cm^{-2}. The V_{oc} temperature dependence of PERL cells was independently measured to be about -1.6 mV K^{-1}. Thus, cell temperatures in Figure 3 are increased by about 0.3°C at 1 sun and about 0.7°C at 2 suns. Below ~0.5 sun, the temperature increase is negligible.

Figure 4 shows the temperature-corrected J_{sc}–V_{oc} curves and the corresponding ideality factors for two cells of Figure 3. The ideality factor of the 2 Ω·cm cell starts at 1.43, reduces to about 1.08 at one sun illumination and decreases slightly below unity at 2 suns. The 10 Ω·cm cell has a much wider voltage range with a constant ideality factor (about 1.4) and significantly lower open-circuit voltages than the 2 Ω·cm cell. Above 630 mV, however, the advantage of the 2 Ω·cm cell begins to decrease, and above 710 mV there is no significant difference between the cells.

Comparison of illuminated and dark I V characteristics

As mentioned above, the measured illuminated I–V curve can be shifted by the short-circuit current density from the fourth into the first quadrant in order to allow for a direct comparison of the illuminated I–V characteristics with the J_{sc}–V_{oc} curve and the dark I–V curve. In Figure 5, this procedure is demonstrated for the 2 Ω·cm cell. Owing to intensity variations of the solar simulator, the plot is restricted to currents larger than 10^{-4} A cm^{-2}. According to Figure 5, the dark I–V curve and the J_{sc}–V_{oc} curve of PERL cells coincide near the AM1.5 maximum power point (voltages of 580–620 mV and currents of 1–2 mA cm^{-2}). At these low currents the impact of the series resistance R_s on the dark I–V curve is negligible. In general, the carrier distributions in a solar cell are significantly different for illuminated and dark I–V conditions. However, Figure 5 indicates that near the maximum power point, the

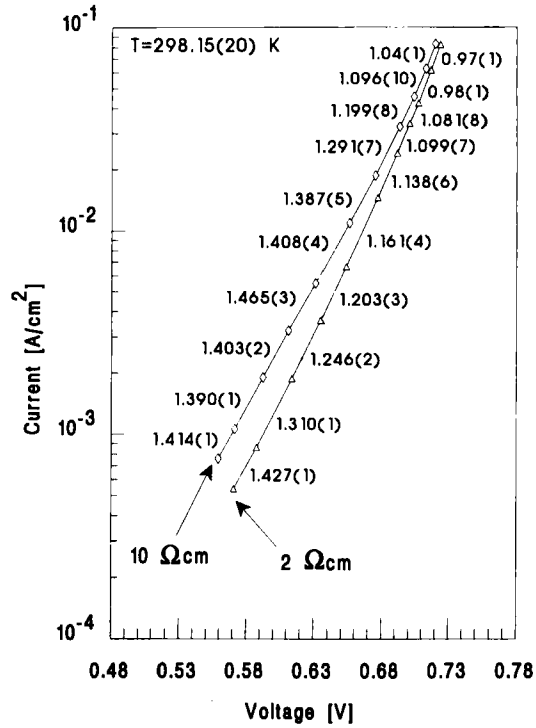

Figure 4. Temperature corrected J_{sc}–V_{oc} characteristics and calculated ideality factors for the 2 and 10 Ω·cm cells of Figure 3

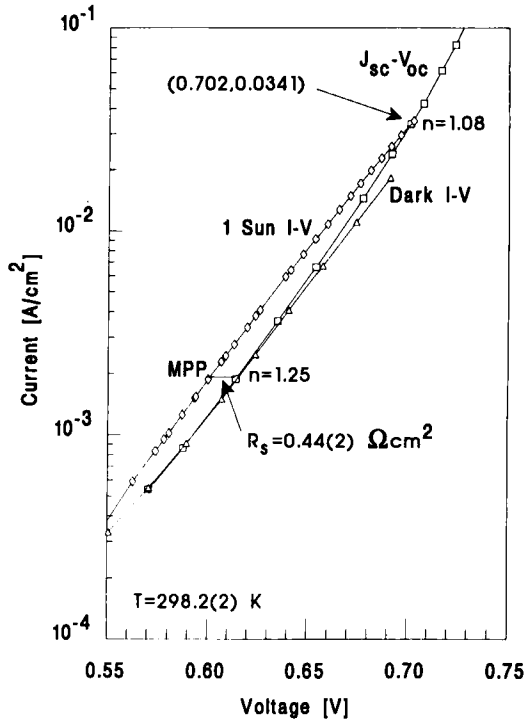

Figure 5. Illuminated 1-sun I–V curve, J_{sc}–V_{oc} curve and dark I–V curve of the 2 Ω·cm cell Wp2-1L

recombination parameters of PERL cells are completely determined by the voltage across the cell. This is a direct result of the large diffusion lengths of PERL cells (several times the wafer thickness), ensuring that for a given voltage across the cell the carrier concentrations at the rear surface are similar for dark and illuminated conditions. Thus, although the J_{sc}–V_{oc} curve was measured for light intensities of 0.01–1.0 sun, it represents a very good approximation to the R_s-corrected 1-sun I–V curve of PERL cells.

Another important result of Figure 5 is that the standard method for the extraction of the series resistance R_s from the dark I–V curve by means of curve fitting cannot be applied to PERL cells owing to the voltage-dependent saturation currents which cause a bending of the J_{sc}–V_{oc} curve towards higher currents at voltages above 700 mV. The most accurate means of determining R_s is from the voltage shift between the illuminated and the dark (or J_{sc}–V_{oc}) curve near the maximum power point. According to Figure 5, cell Wp2-1L has a series resistance of 0.44(2) $\Omega \cdot cm^2$ near the maximum power point. This relatively large value for a high-efficiency 1-sun solar cell arises from the light emitter doping and the rear contact scheme of PERL cells (the latter leading to losses due to rear contact resistance and lateral resistance in the base).

ORIGIN OF NON-IDEAL DIODE BEHAVIOUR

The base of PERL cells is separated by a passivating silicon dioxide layer from the rear aluminium electrode and forms a metal-oxide-semiconductor (MOS) system (Figure 1). Contact to the base is restricted to small (10 μm × 10 μm), widely spaced (250 μm) point contacts sitting on p^+-diffusions (30 µm squares) forming a local back-surface field. The point diffusions cover about 1.8% and the point contacts about 0.2% of the rear surface.

The origin of the non-ideal diode behaviour of PERL cells is a surface recombination velocity S at the rear Si–SiO_2 interface that strongly depends on the minority carrier concentration or, equivalently, on the voltage across the cell.[4,5] Owing to work function differences in the Si–SiO_2–Al system and the positive fixed oxide charge density Q_f typically found at thermally oxidized silicon surfaces,[6] depletion conditions prevail at the rear silicon surface at thermal equilibrium. By applying a voltage or shining light on the cell, the minority carrier concentration at the rear surface increases by several orders of magnitude, and surface band bending as well as surface recombination rates are significantly modified. The measured ideal dark I–V characteristics at voltages below 400 mV (see Figure 2) exclude other possible explanations (e.g. depletion region recombination or edge effects) as the origin of the observed non-ideal diode behaviour.

The impact of light-induced charge carrier concentration on recombination rates at the Si–SiO_2 interface was theoretically and/or experimentally investigated by several research groups.[7–18] Probably the most comprehensive theoretical and experimental work addressing the effect of surface potential, oxide parameters and illumination level upon recombination losses at the rear Si–SiO_2 interface of silicon solar cells was recently performed by Aberle *et al.*[15] In this work it was experimentally verified that with increasing minority carrier concentration at the rear of n^+p bifacial solar cells passivated by a high-quality thermal oxide, the surface recombination velocity decreases by several orders of magnitude to values below 50 cm s^{-1} at AM1.5 illumination. This strong dependence results from the measured asymmetry of the electron and hole capture cross-sections ($\sigma_n/\sigma_p = 10^2$–10^3 near midgap) at the investigated oxidized silicon surfaces and the depletion condition below the surface built up by positive fixed oxide charges Q_f ($\sim 1 \times 10^{11}$ charges cm^{-2}). Owing to the coverage by Al, the depletion condition in the silicon introduced by the work function difference of the Si–Al system has to be taken into account in the modelling of PERL cells. Computer simulations based on energy-resolved measurements of the interface state density, the capture cross-sections of electrons and holes and the fixed oxide charge density show that for an oxide thickness of 1050 Å, surface recombination velocities below 1 cm s^{-1} are obtainable at the rear Si–SiO_2 interface of PERL cells at the AM1.5 maximum power point.[15,16]

Qualitatively, the strong dependence of S on carrier concentration at the rear Si–SiO_2 interface of n^+p PERL cells can be explained by the superposition of two independent mechanisms causing similar results.

Firstly, as can be seen from simple flatband Shockley–Read–Hall (SRH) theory for midgap traps, the large asymmetry in the capture cross-sections ($\sigma_n \gg \sigma_p$) leads to a strong decrease of S once the injection level in p-type material exceeds a critical value.[18] Furthermore, this decrease begins when electron concentrations are several orders of magnitude below the background doping density.[18] This transition is easily reached by PERL cells at 1-sun operating voltages. It is fundamentally due to a transition from recombination limited by the capture of electrons to that limited by the capture of holes.

The second mechanism arises from the depletion condition introduced by the positive oxide charges and the Si–Al work function difference. To gain insight into this mechanism, the simplified case of midgap traps and equal electron and hole capture cross-sections is discussed here. At small voltages, the capture of minority carriers (electrons) is the rate-limiting step in the SRH recombination process. The surface electron concentration is much larger than that of the bulk owing to the surface band bending. The surface recombination velocity is greater than the low-level injection flatband value, S_0, by the ratio of surface to bulk electron concentration. At intermediate voltages, when the surface carrier concentrations become comparable in magnitude, the above ratio decreases, as does the surface recombination velocity. Finally, when the bulk goes into high injection, the capture of electrons and holes equally affects the surface recombination process, and S approaches its normal high-injection flatband value of $S_0/2$. This mechanism basically arises from high-injection effects, with high injection occurring first at the surface and then in the bulk owing to the band bending.

At a real silicon surface the situation is more complex. These two basic mechanisms are modified by the continuum of surface states and the energy dependence of the capture cross-sections.

Owing to the voltage dependence of the rear Si–SiO_2 interface recombination, the base saturation current J_{0b} of PERL cells is not a constant but depends on the cell voltage, causing the observed non-ideal diode behaviour for intermediate voltages. Assuming a constant emitter saturation current with unity ideality factor for voltages below 700 mV, the dashed line in Figure 3 indicates that the base contribution to the total saturation current density increases with reducing cell voltage. At the maximum power point, the base contribution to the total saturation current is at least 44% for the 2 Ω·cm cell, 56% for the 1 Ω·cm cell and 68% for the 10 Ω·cm cell. These values indicate that at the AM1.5 maximum power point the surface recombination velocity at the rear Si–SiO_2 interface has strongly increased from its value at V_{oc} conditions and rear surface recombination losses play an important role in limiting cell efficiency. This difference from the modelling predictions of Aberle *et al.*[16] partly results from the very large oxide thickness of the UNSW cells (>3000 Å), which significantly reduces the positive impact of the Al work function owing to the larger potential drop across the oxide. Another reason could be different oxide parameters at UNSW (e.g. a smaller amount of positive fixed oxide charges Q_f or a modified energy dependence of capture cross-sections for electrons and holes).

Neglecting any two- or three-dimensional effects introduced by the rear point contacts and the front fingers of the cells, the measured dark I–V curves of Figure 2 can be modelled with the numerical one-dimensional solar cell simulator PC-1D.[19] For this PC-1D study we assumed the flatband condition model at the surface and neglected recombination in the emitter as well as at the rear point contacts, so that the resulting S-values can be regarded as an upper limit for the surface recombination velocity at the rear Si–SiO_2 interface. Figure 6 shows the resulting data, which are based on the recently published value of $1.00(3) \times 10^{10}$ cm^{-3} for the intrinsic carrier concentration in silicon at 300 K,[20] and the radiative recombination constant $B = 9.5 \times 10^{-15}$ cm^3 s^{-1}.[21] With increasing voltage, the rear surface recombination velocity drops from very high values (above 10^4 cm s^{-1}) to values in the 15–50 cm s^{-1} range. The higher the base resistivity, the earlier the transition from high to low S-values occurs. Near 630 mV (carrier concentrations comparable to maximum power point conditions at AM1.5 illumination), the higher resistivity cells have reached a minimum S-value (the slight increase in S for the 10 and 100 Ω·cm cells is attributed to high injection conditions in the base[7]), while the surface recombination velocity of the 1 Ω·cm cell has not yet reduced sufficiently. The lowest S-values at the AM1.5 maximum power point are obtained on the 2 Ω·cm substrate. The behaviour of the 1 Ω·cm cell is in agreement with other experiments showing a strong S-increase at SiO_2-passivated p-type silicon surfaces for boron concentrations above 10^{16} cm^{-3}.[5,9]

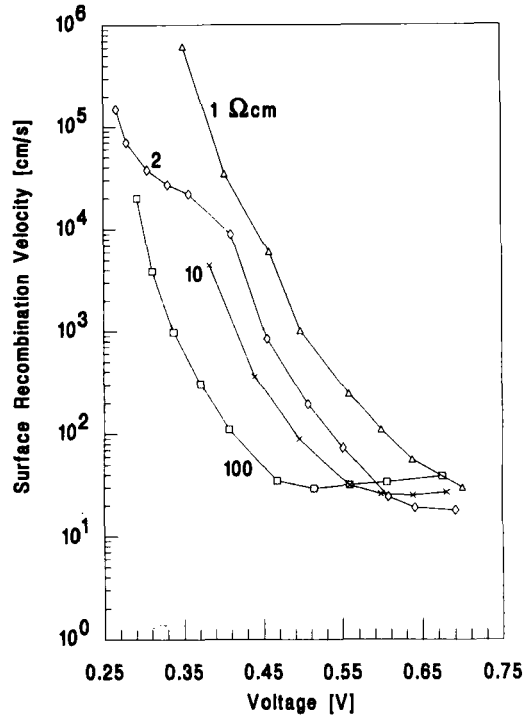

Figure 6. Upper limit of the surface recombination velocity at the rare Si–SiO_2 interface of n^+p PERL cells as a function of the dark I–V cell voltage (calculated from the dark I–V curves of Figure 1 using the numerical device simulator PC-1D)

Figure 7 shows the recombination components in a 2 Ω·cm PERL cell as a function of light intensity. The curves were calculated with PC-1D on the basis of the rear surface recombination velocities of Figure 6. The following parameters were assumed: n^+p cell with planar front surface, Gaussian emitter (surface concentration 3×10^{18} cm^{-3}, junction depth 0.75 μm), cell thickness 280 μm, 25°C, front surface recombination velocity 2000 cm s^{-1}, SRH low injection lifetime 2 ms. Apart from the intrinsic carrier concentration n_i (1.0×10^{10} cm^{-3}) and the radiative recombination constant B (9.5×10^{-15} cm^3 s^{-1}), the default parameters of PC-1D were assumed. As recombination at metal contacts is neglected, the surface recombination losses in Figure 7 represent lower limits for the total surface losses in actual PERL cells. The figure indicates that at the 1-sun open-circuit voltage the front surface is the dominant contributor, while at the 1-sun maximum power point (i.e. at $\sim 2 \times 10^{-2}$ suns in Figure 7) recombination losses primarily occur at the rear surface. Experimental evidence for the V_{oc}-limiting role of the front surface at 1-sun illumination is reported by Zhao *et al.*[22] By depositing positive charges on the top surface of PERL cells, a V_{oc} improvement of up to 10 mV is observed at AM1.5 illumination. Assuming a unity ideality factor, this improvement indicates that at 1-sun open-circuit conditions recombination at the top surface is significant and that the unmetallized emitter region contributes at least 33% to the total saturation current.

SERIES RESISTANCE-CORRECTED EFFICIENCY AND FILL FACTOR

Table I summarizes the parameters of the four planar PERL cells investigated in the previous sections and a 1 Ω·cm PERL cell with inverted pyramids on the emitter surface. The values in parentheses are

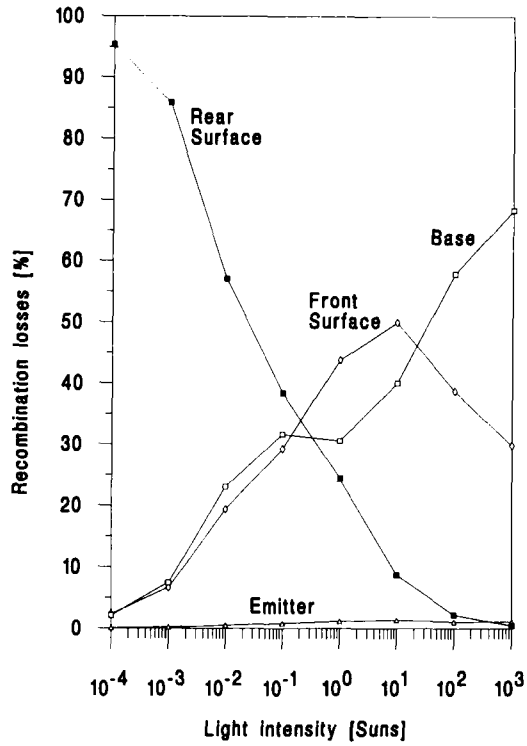

Figure 7. PC-1D calculations of recombination components at open-circuit conditions in a 2 Ω·cm PERL cell as a function of light intensity

Table I. AM1.5 parameters of n^+p PERL cells (25°C, unscribed cells, cells measured with a 20 mm × 20 mm shading mask). The values in parentheses are the R_s-corrected parameters as obtained from the J_{sc}–V_{oc} curves; n is the ideality factor and the maximum power point is given by V_{MPP}, J_{MPP})

Cell	A100-1R	Wp10-1L	Wp2-1L	Wp1-1R	Wt13-R
Resistivity (Ω·cm)	100	10	2	1	1
Front surface	Planar	Planar	Planar	Planar	Inverted Pyramids
R_s(Ω·cm^2)	0.61	0.46	0.44	0.73	0.35
n near V_{oc}	1.24	1.20	1.08	1.00	1.06
n near MPP	1.74	1.39	1.31	1.53	1.50
J_{sc} (mA cm^{-2})	34.90	33.81	34.09	33.40	39.47
V_{oc} (mV)	690.8	695.7	702.3	704.2	698.8
FF (%)	75.21 (78.73)	78.49 (80.35)	81.38 (82.84)	78.16 (81.44)	79.63 (81.36)
η (%)	18.13 (18.98)	18.46 (18.90)	19.48 (19.83)	18.38 (19.15)	21.96 (22.44)
V_{MPP} (mV)	569 (586)	582 (592)	597 (618)	589 (610)	588 (602)
J_{MPP} (mA cm^{-2})	31.86 (32.39)	31.72 (31.92)	32.63 (32.09)	31.21 (31.39)	37.35 (37.28)

the series resistance-corrected parameters of the cells as obtained from the J_{sc}–V_{oc} curves. Owing to the voltage-dependent rear surface recombination velocity, R_s-corrected fill factors are found to be limited to values below 82.9% for the 2 Ω·cm cell, 81.5% for the 1 Ω·cm cells and 80.4% for the 10 Ω·cm cell. Additional reductions in fill factors to the experimentally observed values beow 81.4% result from relatively large values for the series resistance R_s (>0.35 Ω·cm^2). Owing to the increased rear surface recombination velocity and the reduction in S above the maximum power point (see Figure 6), the

1 Ω·cm cell shows no advantage in open-circuit voltage and has a lower fill factor potential than the 2 Ω·cm cell.

The best parameter for the assessment of recombination losses near the maximum power point is the corresponding R_s-corrected voltage V_{MPP} of the cell. The current density J_{MPP} is not a comparable quantity as it is strongly affected by reflection losses at the illuminated front surface. Table I shows that the highest R_s-corrected V_{MPP} (618 mV) results from the 2 Ω·cm cell, followed by the 1 Ω·cm cells Wp1-1R (610 mV) and Wt13-R (602 mV). With increasing base resistivity, V_{MPP} drops significantly (592 mV for 10 Ω·cm; 586 mV for the 100 Ω·cm cell). According to Table I, the dominant parameter determining the optimum wafer resistivity of PERL cells is the rear surface recombination velocity obtainable at the maximum power point and the corresponding impact on V_{MPP}. With increasing resistivity, PERL cells have higher short-circuit currents owing to increased diffusion lengths. However, this advantage is overcompensated by the increase in the cell series resistance, the loss in cell voltage and the high ideality factor leading to small fill factors. Thus, even if series resistance losses are neglected, the high resistivity cells of Table I cannot compete with the 2 Ω·cm cell. On the other hand, owing to increased rear surface recombination velocity, low-resistivity cells do not show increased cell voltages but suffer from current losses. As a consequence, 2 Ω·cm cells presently yield the highest AM1.5 efficiencies.

CONCLUSIONS

The experimentally observed low fill factors of PERL cells at AM1.5 illumination result from an improving surface recombination velocity at the rear Si–SiO_2 interface with increasing voltage across the cell, leading to I–V curves with high ideality factors (>1.3) near the maximum power point. The R_s-corrected fill factors are found to be limited to values below 82.9% for 2 Ω·cm cells, 81.5% for 1 Ω·cm cells and 80.4% for 10 Ω·cm cells, respectively. Relatively large series resistance losses ($R_s > 0.35\ \Omega\cdot cm^2$) further reduce these values to the experimentally observed fill factors below 81.4%.

Optimum wafer resistivity for PERL cell processing is found to be about 2 Ω·cm. Owing to increased rear surface recombination velocities, lower resistivity material shows no advantage in open-circuit voltage, suffers from short-circuit current losses and, as a result of the stronger reduction in S above the maximum power point, has a lower fill factor potential than the 2 Ω·cm substrate. On the other hand, high-resistivity cells show improved currents but suffer from voltage and fill factor losses.

Generally, the performance of solar cells is assessed by the three parameters short-circuit current density, open-circuit voltage and fill factor. An increase in V_{oc} is commonly believed to lead to a correspondingly improved cell efficiency. This work shows that PERL cells do not follow this simple rule, as the AM1.5 open-circuit voltage is strongly affected by emitter recombination losses, while the maximum power point is mainly determined by recombination losses at the rear oxidized surface. As a consequence, an improvement of emitter properties resulting in an increased V_{oc} is accompanied by a reduction in fill factor, with efficiency remaining nearly unchanged.

A disadvantage of n^+p PERL cells is a significantly reduced efficiency at low light intensities (well below 0.1 sun), as the effectiveness of the rear surface passivation scheme depends on the presence of large minority carrier concentrations in the base. With increasing light concentration, however, rear surface recombination velocity reduces by several orders of magnitude and cell efficiency increases much stronger than would be expected from standard cell theory, resulting in record-high efficiencies at AM1.5 illumination.

The reduction of surface recombination losses at the rear Si–SiO_2 interface is one of the key parameters for future efficiency improvements of PERL solar cells. Possible experimental work includes the use of thicker wafers (reducing the impact of the rear surface upon the base saturation current and slightly increasing the electron concentration at the rear surface at the maximum power point), the incorporation of additional positive oxide charges (e.g. by lowering the oxidation temperature), the incorporation of a floating n^+-emitter at the rear, further improvements in the interface state density D_{it}, or the incorporation of a rear gate electrode as recently reported elsewhere.[15] Furthermore, series resistance losses have to be reduced by the incorporation of larger rear point contacts and a higher emitter doping.

Acknowledgements
Portions of this work were supported by the Energy Research and Development Corporation, the Australian Research Council and Sandia National Laboratories. The Centre for Photovoltaic Devices and Systems is supported by the Australian Research Council Special Research Centres Scheme and Pacific Power. One of the authors (A.G.A.) gratefully acknowledges the support of a Feodor Lynen Fellowship provided by the German Alexander von Humboldt Foundation.

REFERENCES

1. A. W. Blakers, A. Wang, A. M. Milne, J. Zhao and M. A. Green, 22.8% efficient silicon solar cell. *Appl. Phys. Lett.* **55**, 1363 (1989).
2. A. Wang, J. Zhao and M. A. Green, 24% efficient silicon solar cells. *Appl. Phys. Lett.* **57**, 602 (1990).
3. M. A. Green, Recent advances in silicon solar cell performance. *Conf. Rec. 10th European Communities Photovoltaic Solar Energy Conference, Lisbon, 1991*, p. 250.
4. M. A. Green, A. W. Blakers, J. Zhao, A. Wang, A. M. Milne, X. Dai and C. M. Chong, *High Efficiency Silicon Concentrator Solar Cell Research*, Report SAND89-7041. Sandia National Laboratories, Albuquerque (1989).
5. A. G. Aberle, W. Warta, J. Knobloch and B. Voss, Surface passivation of high efficiency silicon solar cells. *Conf. Rec. 21st IEEE Photovoltaic Specialists Conference, Orlando, 1990*, p. 233.
6. S. M. Sze, *Physics of Semiconductor Devices*, 2nd Edn., Wiley, New York (1981).
7. W. D. Eades and R. M. Swanson, Calculation of surface generation and recombination velocities at the Si–SiO_2 interface. *J. Appl. Phys.* **58**, 4267 (1985).
8. E. Yablonovitch, R. M. Swanson, W. D. Eades and B. R. Weinberger, Electron–hole recombination at the Si–SiO_2 interface. *Appl. Phys. Lett.* **48**, 245 (1986).
9. R. R. King, R. A. Sinton and R. M. Swanson, Low surface recombination velocities on doped silicon and their implications for point contact solar cells. *Conf. Rec. 19th IEEE Photovoltaic Specialists Conference, New Orleans, 1987*, p. 1168.
10. R. B. M. Girisch, R. P. Mertens and R. F. de Keersmaecker, Determination of Si–SiO_2 interface recombination parameters using a gate-controlled point-junction diode under illumination. *IEEE Trans. Electron Devices* **ED-35**, 203 (1988).
11. M. A. Green, A. W. Blakers, J. Zhao, A. M. Milne, A. Wang and X. Dai, Characterization of 23-percent efficient silicon solar cells. *IEEE Trans. Electron Devices* **ED-37**, 331 (1990).
12. R. R. King, R. A. Sinton and R. M. Swanson, Studies of diffused phosphorous emitters: saturation current, surface recombination velocity, and quantum efficiency. *IEEE Trans Electron Devices* **ED-37**, 365 (1990).
13. T. Saitoh and H. Hasegawa, Computer analysis of surface recombination velocity for high efficiency single crystalline solar cells. *Conf. Ref. 5th Int. Photovoltaic Science and Engineering Conference, Kyoto, 1990*, p. 579.
14. R. R. King and R. M. Swanson, Studies of diffused boron emitters: saturation current, bandgap narrowing, and surface recombination velocity. *IEEE Trans. Electron Devices* **ED-38**, 1399 (1991).
15. A. G. Aberle, S. Glunz and W. Warta, Impact of illumination level and oxide parameters on Shockley–Read–Hall recombination at the Si–SiO_2 interface. *J. Appl. Phys.* **71**, 4422 (1992).
16. A. G. Aberle, S. Glunz and W. Warta, Field effect passivation of high efficiency silicon solar cells. *Solar Energy Mater. Solar Cells*, accepted for publication.
17. J. Zhao, A. Wang, A. G. Aberle, S. R. Wenham and M. A. Green, 717 mV open-circuit voltage silicon solar cells. *Conf. Rec. 11th European Communities Photovoltaic Solar Energy Conference, Montreux, October 1992*, to be published.
18. J. Knobloch, A. G. Aberle, W. Warta and B. Voss, Dependence of surface recombination velocities at silicon solar cell surfaces on incident light intensity. *Conf. Rec. 8th European Communities Photovoltaic Solar Energy Conference, Florence, 1988*, p. 1165.
19. P. A Basore, Numerical modeling of textured silicon solar cells using PC-1D. *IEEE Trans. Electron Devices* **ED-37**, 337 (1990).
20. A. B. Sproul and M. A. Green, Improved value for the silicon intrinsic carrier concentration from 275 to 375 K. *J. Appl. Phys.* **70**, 846 (1991).
21. H. Schlangenotto, H. Maeder and W. Gerlach, Temperature dependence of the radiative recombination coefficient in silicon. *Phys. Status Solidi A* **21**, 357 (1974).
22. J. Zhao, A. Wang and M. A. Green, unpublished results.